Soft Matter

www.rsc.org/softmatter

Volume 8 | Number 43 | 21 November 2012 | Pages 11007–11194

ISSN 1744-683X

RSC Publishing

PAPER

Rico F. Tabor *et al.*

Compound sessile drops

1744-683X(2012)8:43;1-5

Soft Matter

Dynamic Article Links

Cite this: *Soft Matter*, 2012, **8**, 11042

www.rsc.org/softmatter

PAPER

Compound sessile drops†

Michael J. Neeson,[ab] Rico F. Tabor,*[bc] Franz Grieser,[bd] Raymond R. Dagastine[bef] and Derek Y. C. Chan[abg]

Received 16th July 2012, Accepted 6th September 2012
DOI: 10.1039/c2sm26637g

Compound drops arise from the contact of three immiscible fluids and can assume various geometric forms based on the interfacial chemistry of the phases involved. Here we present a study of a new class of compound drops that is sessile on a solid surface. The possible geometries are demonstrated experimentally with appropriate fluid combinations and accounted for with a quantitative theoretical description. Although such systems are broadly controlled by relative interfacial energies, subtleties such as the van der Waals force and effects of micro-gravity, despite drop sizes being well below the capillary length, come into play in determining the equilibrium state that is achieved. The drying of a compound sessile drop was measured experimentally, and the process revealed a novel transition between different characteristic configurations of compound sessile drops. Such drops may prove to be useful as the first step towards development of functional surfaces in applications such as soft optics, photonics and surface encapsulation.

1 Introduction

Compound or multiphase drops are comprised of two (or more) immiscible fluid drops that share an interface with one another, surrounded by a third, mutually immiscible fluid. In the case of free drops surrounded by a liquid, they are often referred to as multiple emulsions,[1] whereas in a continuous vapour phase they are aerosol droplets. Such drops exist in areas as diverse as multiphase processing, biological interactions within cells and atmospheric chemistry. The geometry of such states at equilibrium is dictated by minimisation of the interfacial energy of the system as a whole.[2] In some cases, one phase may be totally engulfed by another, whereas in others, a nonspherical geometry may result, recently termed 'Janus droplets'.[3,4] Such systems are further complicated by the possibility of local minima in interfacial energy states causing history-dependent geometries to become available, particularly if surface forces are involved in the assembly of drops to form compound bodies. The concept of multiphase droplet systems has been of interest, initially as a curiosity[5] for almost a hundred years, but recent developments in droplet handling have re-kindled research into these compound drops.[6–8]

Multiple emulsions, a special case of compound drops where the internal phase is entirely engulfed by an outer droplet,[1,9] have gained considerable attention due to their potential uses in functionalised foods, pharmaceutical formulations and drug delivery vehicles.[10] The advent of microfluidics has provided a particularly adventitious platform for generating multiple emulsions under well-controlled conditions, providing highly monodisperse and regular systems for synthesis of core–shell particles, for instance, and in other applications.[6–8]

The theoretical description of such multiphase systems shares similarities with the case of a floating liquid lens at the air–water interface.[11–13] A large number of studies have dealt with this problem experimentally and theoretically. A complete description of lenses at planar fluid interfaces has been given by Aveyard and Clint.[11] However, by adding curvature to the supporting interface, such as a lens on a droplet or a similar configuration, additional complexity arises. Of the few available studies that considered such systems, invariably the case of free drops has been considered, wherein the compound drops are entirely surrounded by the continuous phase fluid.[3,14–17] In such a scenario, describing the geometry of equilibrium states becomes a comparatively simple solution of the Young–Laplace equation that accounts for the relative energies of the interfaces and drop volumes.

In this paper, we present a new class of small compound drops that are immobilised on planar solid substrates. The equilibrium drop shapes are now complicated by the drop–substrate

[a]*Department of Mathematics and Statistics, University of Melbourne, Parkville 3010, Australia*
[b]*Particulate Fluids Processing Centre, University of Melbourne, Parkville 3010, Australia*
[c]*School of Chemistry, Monash University, Clayton 3800, Australia. E-mail: rico.tabor@monash.edu; Fax: +61 3 9905 4597; Tel: +61 3 9905 4558*
[d]*School of Chemistry, University of Melbourne, Parkville 3010, Australia*
[e]*Melbourne Centre for Nanofabrication, 151 Wellington Road, Clayton 3168, Australia*
[f]*Department of Chemical and Biomolecular Engineering, University of Melbourne, Parkville 3010, Australia*
[g]*Faculty of Life and Social Sciences, Swinburne University of Technology, Hawthorn 3122, Australia*

† Electronic supplementary information (ESI) available: Ancillary results and videos of evaporating drops on different substrates. See DOI: 10.1039/c2sm26637g

contacts, and hence a larger range of geometries can exist depending on the surface chemistry of the solid–fluid and fluid–fluid interfaces involved, as well as the volume ratios and density differences of phases. In our regime of interest, the dimensions of the drops are well below their capillary length, so the shapes of the interfaces are unaffected by gravity. Nonetheless, because of differences in fluid densities, micro-gravity effects still play a role in determining the minimum energy configurations of such compound sessile drops. Indeed, this is a unique circumstance wherein van der Waals forces of quantum mechanical origin compete with the gravitational force to determine soft structures on a micro- to nano-scale. A theoretical model is developed that can account for the geometries that are observed experimentally and that offers insight into 'design rules' for obtaining compound sessile drops from common material combinations. By observing the evaporation dynamics of a compound water/mercury drop on a surface, competition between fluid–fluid and fluid–solid interfacial energies is seen, the balance of which determines the configuration of the compound drop. Such drops may have interesting properties as tuneable micro-lenses for the modification of interfacial photonic properties, as well as providing a unique system to interrogate evaporation dynamics, which is fundamental to the novel technique of evaporative lithography.[18,19]

Herein, we give a brief description of possible compound sessile drops on a planar substrate and introduce the theoretical framework required to provide quantitative descriptions of such drops in Section 3. Examples of experimental realisations of different characteristic compound sessile drops are given in Section 4. These are chosen to be at key locations of the drop parameter phase diagram that would be useful in the design of specific drop configurations. We also explore compound drops where one liquid phase can evaporate and, in doing so, cause a transition between two pseudo-equilibrium drop configurations. Additional experimental results and ancillary details are given in the ESI.†

2 Materials and methods

Water was obtained from a Milli-Q system (minimum resistivity 18.2 MΩ cm). Perfluorooctane (PFO), tetradecane (TD) and 1-bromodecane (BD), all 99% purity, were obtained from Sigma and purified by column chromatography over silica (Florisil, also from Sigma). Mercury metal (99.9%) was obtained from Sigma and used as received.

Experiments were arranged and observed using an inverted microscope (Nikon TE-2000), and images from the side were obtained by using a 1.5 mm right-angle prism (MCPH-1.5, Tower Optical) that was placed on the substrate. Diffuse illumination was provided using a white LED light source and a diffuser. This setup allowed visualisation of drops from either a side-on perspective or from below by simply changing the focus position of the microscope. Drops were formed on three types of glass substrates that were functionalised to provide desired surface chemical properties: (i) treatment in 10% HNO_3 rendered the glass highly *hydrophilic* (water contact angle in air < 10°); (ii) boiling in ethanol for 4 hours made them *semi-hydrophobic* (water contact angle in air ≈ 20°) and (iii) immersion in a 1% OTS solution in heptane for 30 minutes made the glass *hydrophobic* (water contact angle in air ≈ 95°). Surface and interfacial tension measurements were carried out using a standard drop-shape tensiometer.

Compound drops were prepared by depositing an initial sessile droplet on the substrate using glass syringes (10 μL, Hamilton Corp.) and then adding another drop or bubble either directly with the syringe or *via* an atomic force microscope (AFM) cantilever. The AFM used was an Asylum Research MFP-3D, and the cantilevers used were especially fabricated to enable facile capture of bubbles and droplets. This process has been described in detail previously[20–22] and so it is not reproduced here. Photographs of the drops were taken using a digital CCD camera, and image analysis and fitting were performed using the Wolfram *Mathematica* software.

3 Theoretical considerations

We consider surface-immobilised compound sessile drops resting on a planar solid substrate as illustrated in Fig. 1. The compound sessile drop comprised of phases 2 and 3 is surrounded by a continuous fluid phase 1 above the substrate. Clearly such configurations are possible only if the three interfacial tensions γ_{ij} satisfy the triangular inequality

$$\gamma_{ij} < \gamma_{jk} + \gamma_{ki} \tag{1}$$

for all cyclic permutations of the indices $\{i, j, k\} = \{1, 2, 3\}$ in order for the 3-phase contact line to form. There are four cases that we will consider.

(a) A small drop is entirely encapsulated within a large sessile drop (Fig. 1a). The small drop is less dense than the sessile phase so that the buoyancy force will position it at the apex of the sessile drop where it is separated from the outer phase by a thin film of the sessile fluid.

(b) A small drop forms a lens on the top of the sessile drop with a three-phase contact line between all three fluids (Fig. 1b). Again, the buoyancy force positions the lighter lens at the apex of the sessile drop. If the lens dimensions are small compared to the radius of the sessile drop, this case is similar to a drop resting on a planar interface studied by Aveyard and Clint.[11]

(c) A sessile drop with an axisymmetric pendular ring or collar of another fluid around it at the base (Fig. 1c).[23]

(d) A sessile Janus drop in contact with the substrate in an asymmetric configuration (Fig. 1d).

The configurations in Fig. 1a–c are axisymmetric. As the case in Fig. 1a does not contain intersecting interfaces, the small inner drop is spherical and the shape of the outer sessile drop is a portion of the spherical cap.

To describe the compound sessile drops in Fig. 1b and c, we identify the interfacial tension γ_{ij} of the ij-interface ($i, j = 1, 2, 3$; see Fig. 2 and 3) and the corresponding capillary length $\lambda_{ij} = \sqrt{\gamma_{ij}/\Delta\rho_{ij}g}$, where $\Delta\rho_{ij}$ is the density difference between the

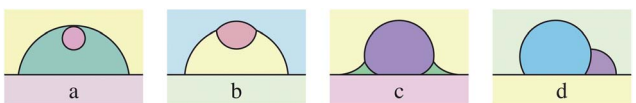

Fig. 1 Configurations of compound sessile drops: (a) encapsulated, (b) lens, (c) collar and (d) Janus drops. The colouring scheme of different phases is simply to provide visual contrast.

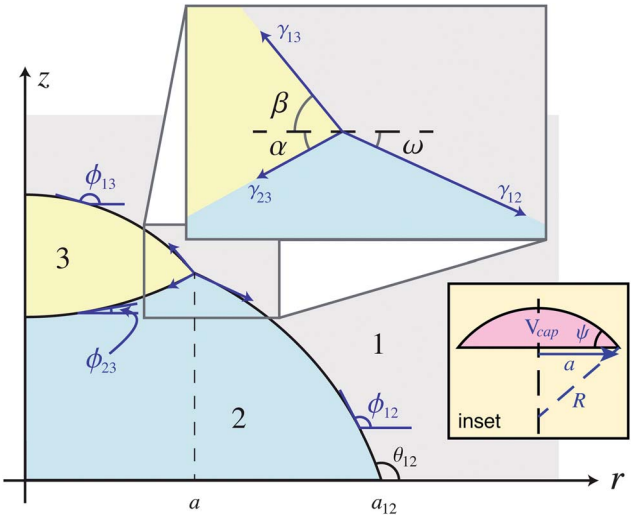

Fig. 2 A schematic representation of the three-phase contact region of a lens on a sessile drop comprising 3 mutually immiscible fluids with interfacial tensions γ_{12}, γ_{23} and γ_{13}. Inset: a spherical cap of volume V_{cap} with a base radius a subtending an angle ψ.

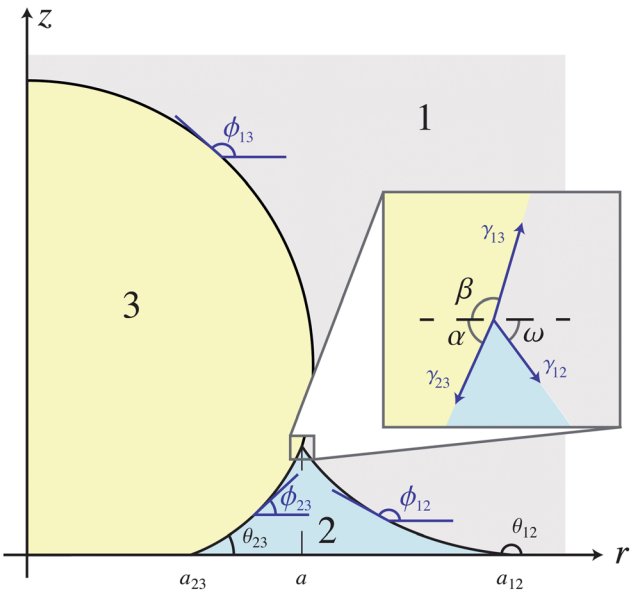

Fig. 3 A schematic representation of the three-phase contact region of a collar around the base of a sessile drop comprising 3 mutually immiscible fluids with interfacial tensions γ_{12}, γ_{13} and γ_{23}.

phases and g is the gravitational acceleration. For the fluid systems we consider here, $\lambda_{ij} \gtrsim 2$ mm, whereas a typical length scale L for the drops we shall consider is $L \simeq 150$ μm, which gives corresponding Bond numbers $B_{ij} \equiv (L/\lambda_{ij})^2 \simeq 0.01 \ll 1$. This implies that the effects of gravity may be omitted when considering the equilibrium shapes of the interfaces of the immiscible fluids in Fig. 1. The shape of each interface is determined by the Young–Laplace equation, which relates the local mean curvature to the pressure difference across the interfaces

$$\gamma_{ij}\left(\frac{1}{R_1}+\frac{1}{R_2}\right) = P_j - P_i \equiv \Delta P_{ij} \tag{2}$$

with R_1 and R_2 representing the principal radii of curvature.

Using cylindrical coordinates, the axisymmetric fluid interfaces in Fig. 1b and c can be described by their height $z(r)$ above the substrate. The Young–Laplace equation for each interface can be written as

$$\frac{\gamma}{r}\frac{\mathrm{d}}{\mathrm{d}r}(r\sin\phi) = \Delta P \equiv \frac{2\gamma}{R} \tag{3a}$$

$$\tan\phi = \frac{\mathrm{d}z}{\mathrm{d}r} \equiv z'(r) \tag{3b}$$

where R denotes the Laplace radius of the interface and ϕ is the tangent angle.

We now derive the boundary conditions for the axisymmetric cases in Fig. 2 and 3.

3.1 Sessile drop with a lens

A detailed view of the axisymmetric compound sessile drop with a lens at the apex is given in Fig. 2. Each of the three interfaces satisfies the Young–Laplace equation, eqn (3), a second order differential equation that requires two boundary conditions plus one further condition to determine the pressure difference, ΔP, or equivalently the Laplace radius, R. Thus all together, 9 conditions are required to determine the shape of the compound sessile drop.

The symmetry conditions of the 12- and 23-interfaces at $r = 0$ and that the 12-interface meets the substrate at a prescribed contact angle θ_{12} at a position $r = a_{12}$ give three conditions

$$z'_{13}(0) = 0 \tag{4a}$$

$$z'_{23}(0) = 0 \tag{4b}$$

$$z'_{12}(a_{12}) = \tan\theta_{12}. \tag{4c}$$

The conditions in eqn (4a) and (4b) imply that the 13- and 23-interfaces are spherical caps of radii R_{13} and R_{23}, respectively. Balancing the components of the interfacial tension in the directions parallel and normal to the 12-interface at the 3-phase contact line at $r = a$ gives two equations that are equivalent to the Neumann triangle condition:

$$\gamma_{13}\cos(\beta - \omega) + \gamma_{23}\cos(\alpha + \omega) = \gamma_{12} \tag{5a}$$

$$\gamma_{13}\sin(\beta - \omega) - \gamma_{23}\sin(\alpha + \omega) = 0. \tag{5b}$$

These equations can be solved to give

$$\cos(\alpha + \omega) = (1 + x^2 - y^2)/2x \tag{6a}$$

$$\cos(\beta - \omega) = (1 + y^2 - x^2)/2y \tag{6b}$$

where $x \equiv \gamma_{23}/\gamma_{12}$ and $y \equiv \gamma_{13}/\gamma_{12}$. Thus, given the interfacial tensions, these equations allow, for example, the angles β and ω to be expressed in terms of α and the interfacial tensions. The value $\alpha = 0$ corresponds to a lens with a planar 23-interface.

Since the change in pressure in crossing the 12- and 23-interfaces is equal to the pressure drop across the 13-interface, we have

$$\Delta P_{12} + \Delta P_{23} = (P_2 - P_1) + (P_3 - P_2) = P_3 - P_1 = \Delta P_{13}.$$

Writing this in terms of the Laplace radii gives

$$\gamma_{12}/R_{12} + \gamma_{23}/R_{23} = \gamma_{13}/R_{13}. \quad (7)$$

In the absence of gravity, the net normal force F exerted by the compound sessile drop on the substrate must vanish. This force is the sum of a downward pressure acting over the base area of the drop and an upward interfacial tension force acting around the perimeter of the base at $r = a_{12}$ where the 12-interface meets the substrate. This condition can be expressed as:

$$\begin{aligned} F &= (\pi {a_{12}}^2)(\Delta P_{12}) - 2\pi a_{12}(\gamma_{12}\sin\theta_{12}) \\ &= 2\pi\gamma_{12}a_{12}\left[\frac{a_{12}}{R_{12}} - \sin\theta_{12}\right] = 0 \end{aligned} \quad (8)$$

and implies that the 12-interface is also a portion of the sphere of radius R_{12} (see ESI†).

Eqn (3)–(6) provide 7 conditions and the final two conditions follow from specifying the volumes of the two phases to be V_2 and V_3. In this configuration, the shapes of all the interfaces are portions of spherical caps. This therefore gives

$$V_2 = a^3\left[\left(\frac{\sin\theta_{12}}{\sin\varpi}\right)^3 v(\pi - \theta_{12}) - v(\omega) \mp v(\alpha)\right] \quad (9a)$$

$$V_3 = a^3[v(\beta) \pm v(\alpha)] \quad (9b)$$

where $V_{cap}(a,\psi) \equiv a^3 v(\psi)$ is the volume of a spherical cap of base radius a subtending an angle ψ (see the inset of Fig. 2) and

$$v(\psi) \equiv \frac{\pi}{3}\,\frac{2 - 3\cos\psi + \cos^3\psi}{\sin^3\psi}. \quad (10)$$

Now given the interfacial tensions, γ_{ij}, the substrate contact angle, θ_{12}, and the drop volumes, V_2 and V_3, eqn (6) and (9) can be solved for a and α. The remaining geometric parameters of the compound sessile drop with a lens are then given by

$$R_{12} = a/\sin\omega,\ R_{23} = a/\sin\alpha,\ R_{13} = a/\sin\beta \quad (11a)$$

$$a_{12} = (\sin\theta_{12}/\sin\omega)a. \quad (11b)$$

3.2 Sessile drop with a collar

The three-phase contact region of a drop with a collar is illustrated in Fig. 3. The 12-interface and the 13-interface meet the substrate at prescribed contact angles θ_{12} and θ_{23} at $r = a_{12}$ and a_{23}, respectively. These together with the symmetry condition at $r = 0$ for the 13-interface gives three conditions

$$z'_{13}(0) = 0 \quad (12a)$$

$$z'_{12}(a_{12}) = \tan\theta_{12} \quad (12b)$$

$$z'_{23}(a_{23}) = \tan\theta_{23}. \quad (12c)$$

The force balance conditions at the three-phase contact line, eqn (6), and the pressure continuity condition, eqn (7), also hold for this case.

For the sessile drop with a collar, both phase 2 and phase 3 exert a downward pressure force on the substrate that can be written as

$$\begin{aligned} F_{\text{pressure}} &= \pi({a_{12}}^2 - {a_{23}}^2)(\Delta P_{12}) + (\pi {a_{23}}^2)(\Delta P_{13}) \\ &= (\pi {a_{12}}^2)(\Delta P_{12}) + (\pi {a_{23}}^2)(\Delta P_{23}) \\ &= 2\pi(\gamma_{12}{a_{12}}^2/R_{12} + \gamma_{23}{a_{23}}^2/R_{23}). \end{aligned}$$

Around the contact lines at $r = a_{12}$ and a_{23} the interfacial tensions exert a upward force

$$F_{\text{interface}} = -2\pi a_{23}(\gamma_{23}\sin\theta_{23}) - 2\pi a_{12}(\gamma_{12}\sin\theta_{12})$$

and these two contributions cancel to give

$$\begin{aligned} F &= F_{\text{pressure}} + F_{\text{interface}} \\ &= 2\pi\gamma_{12}a_{12}\left[\frac{a_{12}}{R_{12}} - \sin\theta_{12}\right] + 2\pi\gamma_{23}a_{23}\left[\frac{a_{23}}{R_{23}} - \sin\theta_{23}\right] = 0. \end{aligned} \quad (13)$$

For the sessile drop with a collar, the 13-interface is a spherical cap due to the boundary condition in eqn (12a), whereas the equations for the 12- and 23-interfaces can be expressed in terms of elliptic integrals. The method of solution is the same as that for the compound sessile drop with a lens given in Section 3.1.

4 Results and discussion

In this section, we demonstrate how the different configurations of compound sessile drops depicted in Fig. 1 can be realised by judicious choice of fluid combinations selected from Table 1. Where possible, the quantitative geometric features of the compound drops are checked against predictions of the Young–Laplace theory and known surface forces that prevail in each system.

4.1 Sessile drop with total encapsulation

An example of a compound sessile drop, radius $\sim$ 150 μm, that contains a fully encapsulated inner phase (see Fig. 1a) is shown in Fig. 4. The perfluorooctane (P) sessile drop is immobilised on a hydrophobic glass substrate and immersed in water (W). The fully encapsulated phase is an air (A) bubble. From the values of interfacial tensions given in Table 1 we see that since

Table 1 Specific gravity (SG), refractive index (RI) and interfacial tensions (γ_{ij}) of fluids used in making compound sessile drops. Interfacial tensions involving mercury are taken from the literature.[24] Other values are measured using the pendent drop method or deduced from the Young–Dupré equation

			γ_{ij}/mN m^{-1}				
SG	RI		BD	M	PFO	TD	W
0.00	1.00	Air (A)	29.5	470	14	—	72
1.07	1.46	Bromodecane (BD)	—	—	—	—	44
13.5	—	Mercury (M)		—	—	—	428
1.77	1.28	Perfluorooctane (PFO)			—	5.4	52.2
0.76	1.43	Tetradecane (TD)				—	47.2
1.00	1.33	Water (W)					—

$\gamma_{AW} > \gamma_{AP} + \gamma_{PW}$, a three phase contact line cannot be formed as it is not possible to satisfy the Neumann triangle condition. As a result, interfacial energies will be minimised when the air bubble is fully encapsulated in the perfluorooctane drop. This is an example of a liquid hydrophobic surface where the surface nanobubble cannot exist as interfacial energy considerations mean that such bubbles will always enter the perfluorooctane phase.

Even though the drop sizes are such that all of the interfaces involved are well below their respective capillary lengths, the bubble is located at the apex of the sessile drop to minimise gravitational energy. Since the refractive index of perfluorooctane (PFO) is intermediate between air and water (see Table 1), a repulsive van der Waals interaction will maintain a thin film of PFO between the air–water and air–PFO interfaces, and hence a disjoining pressure in the oil film balances the buoyancy force. This van der Waals repulsion inferred from refractive index differences has been verified with calculations based on the Lifshitz theory that includes electromagnetic retardation effects.[21] The presence of this film is evident as it is sufficiently thin to give rise to visible interference fringes when illuminated with monochromatic light. The repulsive van der Waals interaction across such films has also been measured directly using an atomic force microscope[25] so here we have an unusual example of a balance between fundamental forces on the nanoscale: van der Waals forces of quantum mechanical origin against gravity.

In the following section, we consider the situation in which the interfacial tensions are able to satisfy the Neumann condition to form a three phase contact line, which gives rise to sessile drops with a lens.

4.2 Sessile drop with a lens

In Fig. 5, we show two characteristic examples of compound sessile drops on a hydrophobic glass substrate under water in which the least dense phase is able to form a floating lens. In each case, this is because the values of the interfacial tensions can satisfy the Neumann condition to form a three phase contact line. In Fig. 5a, we show an air bubble that forms a lens at the apex of a bromodecane drop and in Fig. 5b, we have a tetradecane lens at the apex of a perfluorooctane drop. These two examples are distinguished by the sign of the curvature of the lens surface inside the sessile drop, giving a biconvex lens for the air–bromodecane case, and a convex–concave lens for the tetradecane–perfluorooctane case. The curvatures are controlled by the relationship between the relative phase volumes and the relative magnitudes of the interfacial tensions that determine the interfacial angles at the three phase contact line, when $r = a$ in Fig. 2.

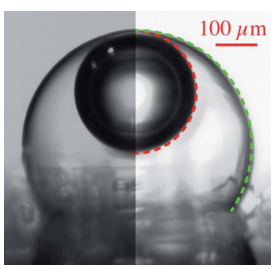

Fig. 4 A compound perfluorooctane sessile drop on a hydrophobic glass substrate in water with a fully encapsulated air bubble. The contrast of the right side of the image has been reduced and the theoretical predictions of the two interfaces are overlaid for comparison.

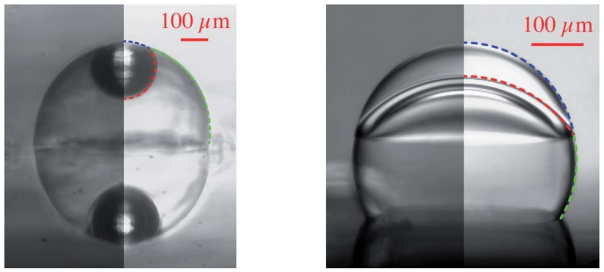

Fig. 5 (a) An air bubble lens in a bromodecane drop on a hydrophobic glass substrate under water. The reflection of the bubble on the glass substrate is visible in the lower half of the photograph. (b) A tetradecane lens on a perfluorooctane drop on a hydrophobic glass substrate under water in which the lens interfaces have opposite curvatures. The contrast of the right side of the images has been reduced and the theoretical predictions of the interfaces are overlaid for comparison.

Again the lens is located at the apex of the sessile drop to minimise the gravitational energy because in each case the density of the lens – air or tetradecane – is less than that of the sessile drop – bromodecane or perfluorooctane – and of the surrounding fluid (in each case water).

The refractive index of the lens (air or tetradecane) is intermediate between that of the sessile drop (bromodecane or perfluorooctane) and water (see Table 1), therefore the van der Waals interactions of the bromodecane–air–water and perfluorooctane–tetradecane–water systems are both attractive. This again favours the formation of three phase contact and the formation of a lens rather than the formation of fully encapsulated drops.

These observations provide simple design rules for creating compound sessile drops with a lens using readily available material properties. The configurations of such compound drops are determined by four parameters: two ratios of the three interfacial energies, $(\gamma_{23}/\gamma_{12})$ and $(\gamma_{13}/\gamma_{12})$, the contact angle on the substrate, θ_{12}, and the volume ratio (V_3/V_2). This paradigm, constructed from eqn (6), is illustrated in the interfacial energy ratio diagram shown in Fig. 6, in terms of the surface energy ratios, $(\gamma_{23}/\gamma_{12})$ and $(\gamma_{13}/\gamma_{12})$, for a base contact angle $\theta_{12} = 90°$ and a volume ratio $V_3/V_2 = 1/4$. Sessile drops with a lens can only form when the surface tension ratios are in the white 'Neumann' region of the diagram where the Neumann condition, eqn (1), can be satisfied. In the grey regions, surface energy minimisation means that phase 3 will exist as a separate phase and form a coating film on phase 2 or be encapsulated in phase 2, as indicated. Characteristic shapes of compound sessile drops with a lens are shown at key points in the energy ratio diagram indicated by the inset figures (i)–(viii). The locations of the experimental compound sessile drops demonstrating encapsulation (Fig. 4) and lens formation (Fig. 5a and b) are also indicated in this diagram. Each contour line in the Neumann region delineates the boundary where the lens is biconcave (to the right) or concave–convex (to the

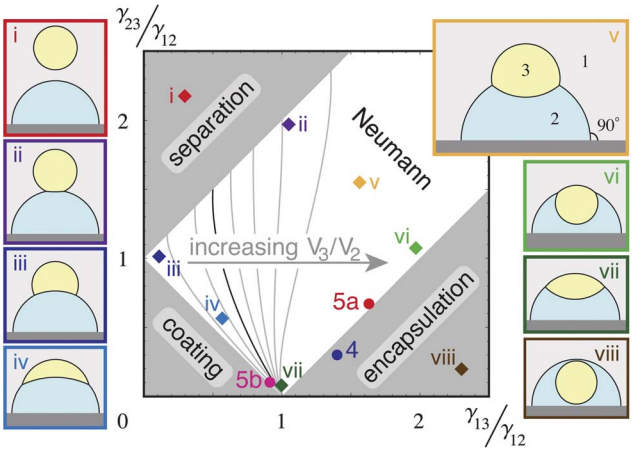

Fig. 6 A representative interfacial energy ratio diagram based on eqn (6) that delineates the domain in which compound sessile drops with a lens can be formed in the Neumann region. The characteristic shapes of the lens in each location of the region are given in the insets (i)–(viii) for the substrate contact angle $\theta_{12} = 90°$ and volume ratio $V_3/V_2 = 1/4$. The locations of the experimental compound sessile drops given in Fig. 4 and 5 are also indicated. The contour lines in the Neumann region locate the boundaries where the lens shape changes from concave–convex (to the left) to biconcave (to the right) at the volume ratios: $V_3/V_2 = 0.01$, 0.1, 0.25, 0.5, 1, 2, and 5. (See text for details.)

left). The location of this boundary varies with the phase volume ratio (V_3/V_2), as indicated.

When the relative densities and interfacial tensions of the fluids favour either the formation of a fully encapsulated drop or a lens on a sessile drop as depicted in Fig. 1, the surface properties of the substrate only determine the contact angle, θ_{12} (see Fig. 2) of the encapsulating drop. However, if the fluid that forms the lens is denser than the surrounding fluid, more complex compound drop configurations can arise. We shall consider these in the following 2 sections.

4.3 Sessile drop with an evaporating collar

When the continuous phase is least dense, as in the case of compound sessile drops in air, both phases of the compound drop can be in contact with the substrate. One possibility for a compound sessile drop under such conditions is the axisymmetric configuration shown in Fig. 1c in which one phase forms a pendular ring or collar around the base of the sessile drop. The outer interface of the collar shares similarities with a liquid meniscus formed when a sphere is held above a surface.[23] A realisation of this configuration using a sessile mercury drop (radius $\sim$ 400 μm) in air on a hydrophilic glass substrate with a water collar around the base of the mercury drop is shown in Fig. 7. The water contact angle on this surface is <10°. The time-lapse sequence of images shows the evaporation of the water collar. Videos of the evaporation of the water collar on a hydrophilic, hydrophobic and a semi-hydrophobic glass substrate are available in the ESI.†

The evaporation in Fig. 7 took about 80 s to complete, and was a quasi-equilibrium process whereby the instantaneous drop and collar shapes can be described accurately by the Young–Laplace equation. In Fig. 8, we give a demonstration of the quasi-

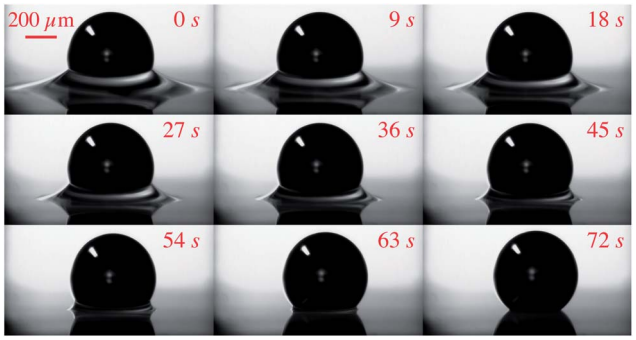

Fig. 7 A mercury drop in air on a hydrophilic glass substrate (water contact angle < 10°) with a water collar around the base. Time-lapse images taken at 9 s apart show the progress of the evaporating water collar. See ESI† for a video.

equilibrium nature of the evaporation of a water collar on a less hydrophilic substrate (water contact angle $\sim$ 30°) by comparing the collar shapes with the predictions of the Young–Laplace equation. Here the evaporation process is slightly slower because the higher water contact angle on the substrate exposes a smaller air–water interface at which evaporation takes place. In both cases, the water collar maintains axisymmetry as it evaporates; there is no apparent tendency for pinning of the air–water contact line on the substrate during evaporation.

The dynamics of the evaporation process can be quantified by analysing the sequence of images. By assuming axial symmetry, the time variations of the collar volume, collar surface area, the Laplace pressure difference across the air–water interface and the contact angles at the substrate have been extracted using the Young–Laplace model and the results are shown in Fig. 9. The rate of evaporation appears to be proportional to the exposed surface area of the evaporating collar, which suggests a dynamic process wherein the drop is not in equilibrium with the saturated vapour phase, but rather the atmosphere is depleted in water

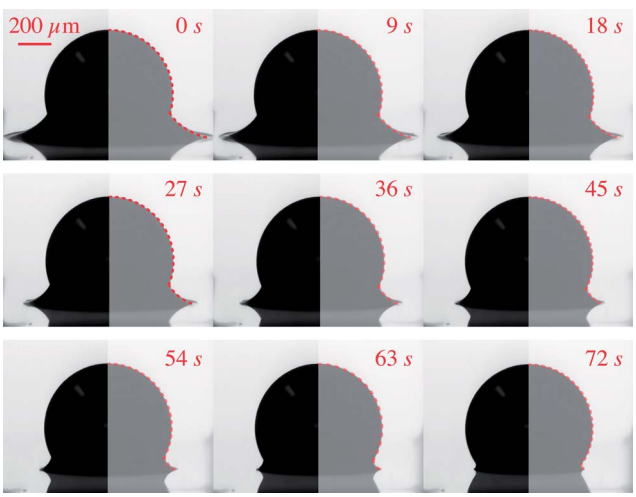

Fig. 8 Time-lapse images of the evolving shapes of a compound sessile drop on a hydrophilic glass substrate that is formed by a mercury drop in air with a water collar around the base (water contact angle $\sim$ 30°). As the water evaporates, successive images of the drop shapes are compared to the predictions of the Young–Laplace equation.

vapour. This is in line with the measured relative humidity within the laboratory (40%). Clearly the interfacial tension forces that act on the collar operate on a timescale that is much shorter than the diffusion driven evaporation process, and hence it is quite reasonable to use the Young–Laplace equation to analyse the drop geometry in each quasi-equilibrium image. It is also evident that the Laplace pressure difference across the air–water interface of the water collar is negative and therefore provides a capillary attraction that pulls the mercury drop towards the substrate. Indeed, towards the end of the evaporation process, small adjustments in the position of the mercury drop are observed as the water collar finally disappears. Videos of evaporation experiments are available in the ESI.†

The results shown in Fig. 9 are likely to be more accurate in the initial 60 s. Thereafter, the volume of the water collar becomes small which increases the uncertainties in the values of the extracted parameters. The relative error in the extracted collar volume is large because the estimation involves the subtraction of quantities of similar magnitude. Within uncertainties in the analysis, the contact angles of the mercury–water interface, θ_{23}, and of the air–water interface, θ_{12}, at the substrate do not vary appreciably during the evaporation process.

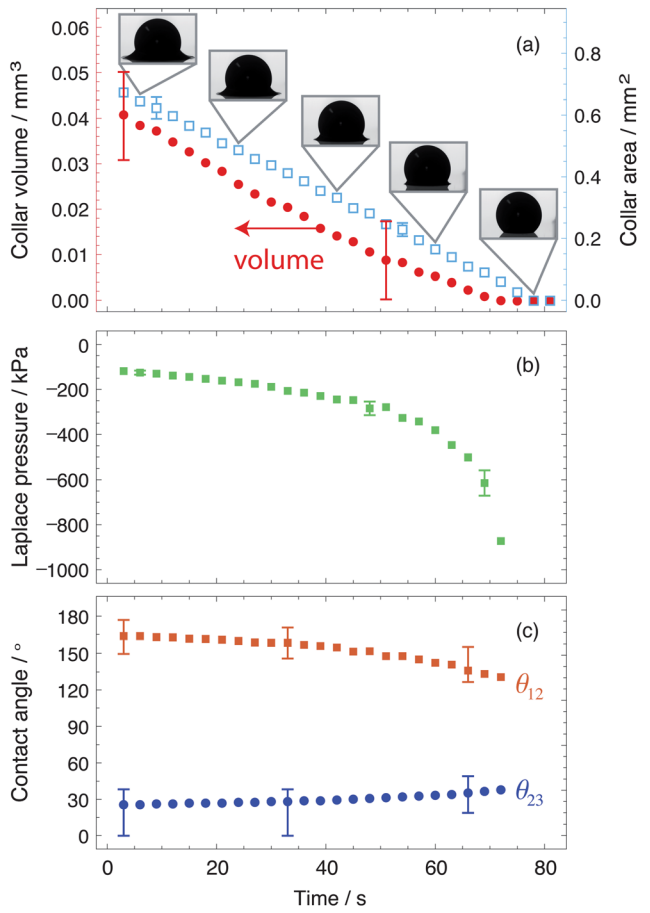

Fig. 9 Time variations of (a) the collar volume (solid symbols, left hand axis) and collar surface area (open symbols, right hand axis), (b) the Laplace pressure of the evaporating water collar and (c) the contact angles of the mercury–water interface, θ_{23}, and of the air–water interface, θ_{12}, at the substrate extracted by fitting the collar shape to solutions of the Young–Laplace equation. Representative error bars are shown in each plot.

In the following section, we will see that collar formation can arise from a complex competition of different interfacial energies and other forces.

4.4 Janus compound drops and collars

The characteristic length scales of all of the compound sessile drops considered so far are significantly below the capillary length. This means that the drop classifications are determined solely by interfacial energies. However, because of density differences between the fluid phases, the drops will adopt the configuration on the substrate that also minimises the gravitational energy. An illustration of this idea is given in Fig. 10a, where a smaller but denser drop is placed on a large sessile drop. In the absence of gravity, the total surface energy of the system does not change as the location of the smaller drop is varied along the surface of the larger drop, provided it does not make contact with the substrate. However, gravity will cause the small drop to slide down and make contact with the substrate. This results in a Janus sessile drop (Fig. 1d).

In Fig. 10b we show an example of a Janus drop in water that is made up of a large mercury drop and a small perfluorooctane drop on a hydrophilic glass substrate. As perfluorooctane is substantially more dense than the surrounding water, gravity dictates that the drop, although placed at the apex of the mercury drop, will slide down until it rests on the substrate. In contrast, for the air–bromodecane–water compound sessile drop shown in Fig. 5a, buoyancy kept the air bubble at the apex of the sessile bromodecane drop. However, if the density of the internal phase is greater than that of the sessile drop and the surrounding fluid, it will slide down to the substrate, as for the mercury–perfluorooctane compound drop, resulting in an asymmetric state.

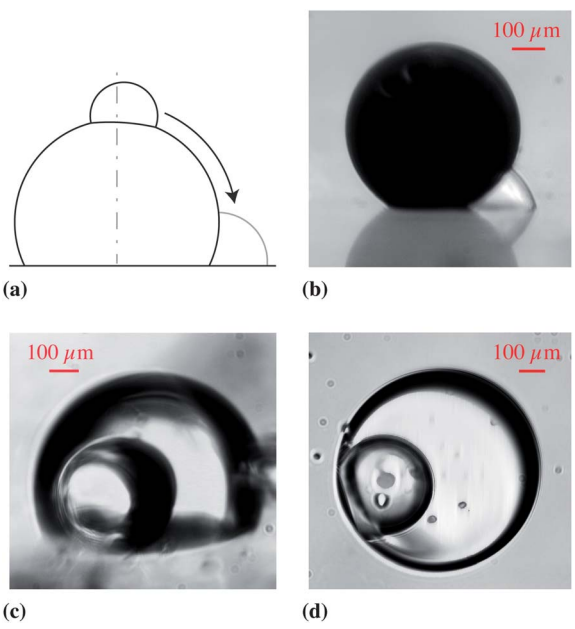

Fig. 10 (a) A dense phase deposited on top of a sessile drop will slide down to contact the substrate to minimise gravitational energy. (b) A Janus sessile drop comprising a small perfluorooctane drop and a large mercury drop in air. (c and d) Two views of a Janus sessile drop in which a perfluorooctane drop appears to reside inside a larger tetradecane drop in water as viewed from the side (c) and from below (d).

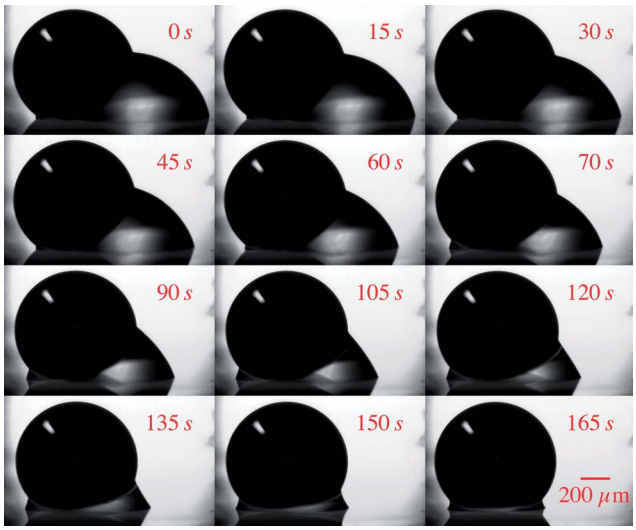

Fig. 11 A mercury–water Janus sessile drop in air on a hydrophobic glass substrate. As the water evaporates, it changes to the collar configuration to maximise the energetically favourable water–mercury (hydrophilic) contact.

An example of this is given in Fig. 10c in which the small perfluorooctane drop of the Janus pair is almost entirely engulfed within the larger tetradecane drop.

An interesting geometric transition occurs if one component of a Janus sessile drop can evaporate. In Fig. 11 we show a mercury–water Janus drop in air that was formed initially on a relatively hydrophobic substrate. The Janus configuration is favoured as it minimises the water–hydrophobic glass contact area although a consideration of Kelvin capillary condensation would suggest that a small water collar around the mercury drop may exist for the initial Janus configuration, even though we cannot resolve it visually. However, as the water evaporates and the water drop volume decreases, the Janus drop undergoes a transition to a sessile mercury drop with a water collar that becomes clearly visible around its base. This occurs because, with a small volume of water, the increase in the energetically favourable water–mercury (hydrophilic) contact area can compensate the energy cost by increasing the water–glass (hydrophobic) contact area. A quantitative analysis of the energetics of such a transition from an asymmetric to an axisymmetric configuration is beyond the scope of the present work; we will address this problem in detail in a separate publication.

5 Conclusions

We have shown that three mutually immiscible fluids can form four different classes of compound sessile drops on a flat substrate. By using common material combinations, we demonstrate that these surface-immobilised compound drops can be realised experimentally in the range of drop-sizes where all interfaces are significantly below the capillary length. As a result, the balance of surface energies dictates the shape of the compound drop adopted. Nonetheless, micro-gravity effects and van der Waals forces also play a role in determining the equilibrium configuration of phases.

Through direct image analysis of experimental drops, we show that the Young–Laplace equation provides an accurate description of the observed drop shapes. The characteristic shapes can be placed in a unified context using an interfacial energy diagram, Fig. 6. This is a useful design tool that can be used to visualise compound sessile drops with a lens with the desired geometric and optical properties.

By studying the evaporation of one component of a Janus sessile drop, an interesting transition was seen from the asymmetric Janus drop to an axisymmetric compound sessile drop with a collar. This transition appears to arise from the balance between the energy gained by increasing the energetically favourable drop–drop contact area against the unfavourable drop–substrate energy. The evaporation dynamics of a purely axisymmetric state were also studied, showing that evaporation was dependent only on the exposed surface area of the evaporating phase. This system may prove to be useful to examine effects such as evaporative self-assembly.

Thus, we have shown that although compound sessile microdrops are comparatively easy to make, a wide range of geometries and behaviours exist. Through careful materials choice and suitable additives, such as styrene or siloxane monomers, drops could be made for applications in soft optics, surface photonics and targeted encapsulation and immobilisation on surfaces.[26]

Acknowledgements

This project is funded in part by the Australian Research Council through a Discovery Project Grant. M.J.N. is supported by an Australian Postgraduate Research Award. The PFPC is thanked for infrastructure support.

References

1 R. E. Johnson and S. S. Sadhal, *Annu. Rev. Fluid Mech.*, 1985, **17**, 280–320.
2 P. G. de Gennes, F. Brochard-Wyatt and D. Quere, *Capillarity and Wetting Phenomena – Drops, Bubbles, Pearls, Waves*, Springer, New York, 2004.
3 J. Guzowski, P. M. Korczyk, S. Jakiela and P. Garstecki, *Soft Matter*, 2012, **8**, 7269–7278.
4 T. Nisisako and T. Torii, *Adv. Mater.*, 2007, **19**, 1489–1493.
5 J. M. Andreas, *J. Chem. Ed.*, 1938, **15**, 523.
6 A. R. Abate and D. A. Weitz, *Small*, 2009, **5**, 2030–2032.
7 Z. Bei, T. B. Jones and D. R. Harding, *Soft Matter*, 2010, **6**, 2312–2320.
8 M. Seo, C. Paquet, Z. Nie, S. Xu and E. Kumacheva, *Soft Matter*, 2007, **3**, 986–992.
9 S. S. Sadhal and H. N. Oguz, *J. Fluid Mech.*, 1985, **160**, 511–529.
10 D.-H. Lee, Y.-M. Goh, J.-S. Kim, H.-K. Kim, H.-H. Kang, K.-D. Suh and J.-W. Kim, *J. Dispersion Sci. Technol.*, 2002, **23**, 491–497.
11 R. Aveyard and J. H. Clint, *J. Chem. Soc., Faraday Trans.*, 1997, **93**, 1397–1403.
12 J. C. Burton, F. M. Huisman, P. Alison, D. Rogerson and P. Taborek, *Langmuir*, 2010, **26**, 15316–15324.
13 C. M. Phan, B. Allen, L. B. Peters, T. N. Le and M. O. Tade, *Langmuir*, 2012, **28**, 4609–4613.
14 M. Aratono, T. Toyomasu, N. Ikeda and T. Takiue, *J. Colloid Interface Sci.*, 1999, **218**, 412–422.
15 Y. Shao and T. G. M. van de Ven, *Langmuir*, 1989, **5**, 1234–1241.
16 O. M. Lavrentevea, L. Rosenfeld and A. Nir, *Phys. Rev. E: Stat., Nonlinear, Soft Matter Phys.*, 2011, **84**, 056323.
17 L. Rosenfeld, O. M. Lavrentevea and A. Nir, *J. Fluid Mech.*, 2009, **626**, 263–289.

18 R. D. Deegan, O. Bakajin, T. F. Dupont, G. Huber, S. R. Nagel and T. A. Witten, *Nature*, 1997, **389**, 827–829.
19 I. U. Vakarelski, D. Y. C. Chan, T. Nonoguchi, H. Shinto and K. Higashitani, *Phys. Rev. Lett.*, 2009, **102**, 058303.
20 R. F. Tabor, F. Grieser, R. R. Dagastine and D. Y. C. Chan, *J. Colloid Interface Sci.*, 2012, **371**, 1–14.
21 R. F. Tabor, C. Wu, H. Lockie, R. Manica, D. Y. C. Chan, F. Grieser and R. R. Dagastine, *Soft Matter*, 2011, **7**, 8977–8983.
22 R. F. Tabor, A. J. Morfa, F. Grieser, D. Y. C. Chan and R. R. Dagastine, *Langmuir*, 2011, **27**, 6026–6030.
23 F. M. Orr, L. E. Scriven and A. P. Rivas, *J. Fluid Mech.*, 1975, **67**, 723–742.
24 M. C. Wilkinson, *Chem. Rev.*, 1972, **72**, 575–625.
25 R. F. Tabor, R. Manica, D. Y. C. Chan, F. Grieser and R. R. Dagastine, *Phys. Rev. Lett.*, 2011, **106**, 064501/1–064501/4.
26 D. Graham-Rowe, *Nat. Photonics*, Sept. 2006, 2–4.

